

Author Manuscript

Title: Covalent Organic Framework as an Efficient Protection Layer for Stable Lithium-metal Anode

Authors: Arumugam Manthiram, Ph.D.; Jiarui He; Amruth Bhargav

This is the author manuscript accepted for publication. It has not been through the copyediting, typesetting, pagination and proofreading process, which may lead to differences between this version and the Version of Record.

To be cited as: 10.1002/anie.202116586

Link to VoR: <https://doi.org/10.1002/anie.202116586>

Covalent Organic Framework as an Efficient Protection Layer for Stable Lithium-metal Anode

Jiarui He, Amruth Bhargav, and Arumugam Manthiram*

[*] Dr. J. He, Mr. A. Bhargav, Prof. A. Manthiram
Materials Science and Engineering Program & Texas Materials Institute
The University of Texas at Austin
Austin, TX 78712, USA
E-mail: manth@austin.utexas.edu (A. Manthiram)
Supporting information for this article is given via a link at the end of the document

Abstract: Lithium (Li) metal shows great potential for achieving high-energy-density rechargeable batteries. However, the practical applications of Li-metal batteries are still challenged by the formation of Li dendrites and unstable solid-electrolyte interphase (SEI) on metallic Li. Herein, a thin covalent organic framework layer is *in-situ* fabricated on Li (COF-Li) to suppress Li dendrite growth and mitigate the side reaction on Li anode. The COF has a periodic and uniform porosity, allowing for selectively sieving Li ions and guiding a uniform Li deposition. As a result, the COF-Li exhibits a non-dendrite morphology during repeated Li plating/stripping and demonstrates a remarkable cycle life over 13,200 h with an extremely low overpotential of only 16 mV at a high current density of 10 mA cm⁻² and a high areal capacity of 10 mA h cm⁻².

Introduction

Electric cars, grid storage, and portable devices all have rising demands, driving the development of high-energy-density batteries.^[1] Lithium metal has received considerable attention due to its attractive characteristics, including a high theoretical capacity (3,860 mA h g⁻¹), a low mass density (0.534 g cm⁻³), and a low reduction potential (-3.04 V vs. standard hydrogen electrode). Lithium metal is a promising anode material for advanced Li-metal batteries (LMBs). It is also an essential component of high-energy unlithiated cathode materials, particularly lithium-sulfur (Li-S) batteries.^[2] However, the unstable solid-electrolyte interphase (SEI) layer continuously forms when the highly reactive Li is exposed to organic electrolytes. During the recurrent stripping and plating process, Li metal experiences huge volumetric changes, followed by a constant shattering of the unstable SEI layer.^[3] The fissures accelerate the growth of regionally concentrated Li-ion flux, which leads to an uneven Li deposition with dendritic morphology that penetrates the separator, causing an internal short-circuit and safety issues.^[4] In addition, the repetitive cracking of the SEI results in a continuous contact between fresh Li and organic electrolyte, which accelerates the consumption of electrolyte and Li, thus reducing the lifespan of batteries.^[5] Therefore, it is critically essential to engineer a stable SEI to achieve high-performance Li-metal batteries.

Several approaches have been developed to protect the lithium-metal anode from the abovementioned issues of unstable SEI and Li dendrite formation, including electrolyte additives, implantable/artificial SEI layer, high concentration electrolyte, solid-state electrolyte, and 3D structured templates.^[6] For example, Guo and co-workers developed a synthetic homogeneous inorganic Li₃PO₄ SEI layer employing an *in-situ* reaction between polyphosphoric acid and lithium metal.^[7]

Zhang and co-workers designed a high concentration electrolyte of 4 M lithium bis(fluorosulfonyl)imide (LiFSI) in 1,2-dimethoxyethane (DME).^[8]

These approaches provided new insights into the preservation of Li metals while also achieving an improved lifespan of batteries. These developed approaches primarily focus on the interface with various chemical compositions. Apart from the interface with the organic and inorganic components, the development of layers with well-designed nanoarchitectures is also essential for suppressing dendritic Li growth and achieving a long lifespan for LMBs. **In addition, the designed artificial SEI, which could selectively sieve Li ions, is also crucial for the LMBs with complex working conditions, such as lithium-sulfur (Li-S) batteries with intensive lithium polysulfide (LiPS) shuttling.**

Herein, we report a thin covalent organic framework (COF) *in-situ* fabricated on Li (COF-Li) as an efficient protection layer for stable LMBs. The COF can prevent Li dendrite growth by selectively sieving Li ions and guiding a uniform Li deposition. The electrochemical performance of COF-Li metal anodes is enhanced with dendrite-free Li deposition in a working battery.

Results and Discussion

Schematic of the synthesis route for COF-Li is shown in Figure 1a, which can be easily fabricated by the drop-casting method based on the co-condensation reaction of diboric acid and hexahydroxytriphenylene (HHTP).^[9] It is noteworthy that this method could be carried out at ambient temperature without any harsh conditions. Aside from that, the unique room temperature vapor-assisted conversion strategy provides a highly scalable coating route that allows for a precise control of the layer thickness. The obtained COF-Li via vapor-assisted reactions at ambient temperature leads to the formation of a light white organic layer on Li foil. In addition, the COFs are connected by robust covalent bonds and thereby show good stability in the organic electrolyte. The top-view scanning electron microscopy (SEM) images in Figures 1b and S1 show that the surface is a homogenous continuous layer with rich nanopores. The observations on the cross-sectional SEM image in Figure 1c indicate a cohesive film with a thickness of approximately 16 μm. **This thin layer of COF-5 provides two distinct benefits. First, the intrinsic pore size of COF-5 is suited for Li-ion conduction. With Li-ion conductivity reported to be around 2.6 × 10⁻⁴ S cm⁻¹,^[10] the COF layer acts as an ion-sieve and ensures a homogeneous Li⁺ flux resulting in uniform metal deposition. Second, the Young's modulus of COF-5 typically ranges from 15-20 GPa which is higher than that of metallic Li (~ 5 GPa).^[11] This makes the COF**

layer strong enough to prevent dendrite growth.^[12] The photograph of the COF-Li in Figure 1d indicates that such a thin coating layer on the Li only slightly influences its visual observation, and the metallic appearance can be seen. The elemental mapping images of the COF-Li in Figure 1e confirm the uniform coating layer of COF on the Li foil.

To further validate the spatial distribution of Li and the elemental composition in COF-Li, time-of-flight secondary ion mass spectrometry (ToF-SIMS) was carried out. As shown in Figure 1f, the depth profiles of the representative secondary-ion species reveal the composition of the COF-Li, including Li_2^+ , C^+ , and BO^+ . Here, Li_2^+ represents metallic Li, and the C^+ and BO^+ are mainly from the COF. The depth profiles of these three species show that their intensities change depending on the sputtering time. After sputtering for 2,700 s, the intensity of the C^+ and BO^+ become negligible while the intensities of Li_2^+ almost reach the maximum value, indicating the coating structure on Li. The 3D visualization of the architecture evolution of the COF-Li in Figure 1g reconfirms the uniform coating structure in COF-Li. To demonstrate our method can easily control the coating layer thickness of COF, we prepared another two COF-Li with different thicknesses by controlling the volume of the BDBA / HHTP solution (Detailed information is provided in the experimental section in supporting information). As shown in Figure S2, an ultrathin layer of COF with a thickness of 5 μm was coated on Li. Unlike the COF with a thickness of 16 μm , the 5 μm thick layer shows a very smooth morphology without any pores on its surface. When the thickness of the COF increases to 51 μm , as shown in Figure S3, the surface constructs with many small intergrown particles endowing a continuous white film with textural porosity on Li foil.

According to the different morphologies of the COF layer with various thicknesses, we can conclude that the coating COF forms a substantial and dense layer close to Li foil with a thickness of approximately 5 μm . Beyond this distance, the COF gradually transforms into a porous architecture. Significantly when the thickness increases to 51 μm , the numerous small intergrown particles can be detected and form a continuous coating layer on the Li foil. Such a unique architecture of COF layer has two advantages. The porous layer far from the Li easily allows for electrolyte penetration and thus ensures a fast Li-ion transport. The solid, dense layer directly contacting Li can effectively protect Li from direct exposure to organic electrolyte and dendrite growth and selectively sieve Li ion, which can be employed in Li-S batteries to prevent LiPS shuttling. Further, the COF structure was also revealed by the FTIR spectra. As shown in Figure S4, the COF-Li is mainly evidenced by the characteristic stretching modes typical for boroxoles: B-O stretching at $1,337\text{ cm}^{-1}$ and C-O stretching at $1,238\text{ cm}^{-1}$,^[9] compared to that of bare Li.

To investigate the Li anode plating/stripping stability of COF-Li, we employed optical microscopy on a Li||Li symmetric cell with a transparent window to visually monitor the Li plating/stripping behavior. As seen in Figure 2a, the photos of the Li cross-sections were obtained at various plating/stripping periods. Both the surface of bare Li and COF-Li at the beginning are smooth. A precise formation of Li dendrites can be observed on the bare Li after plating/stripping at $5\text{ mA cm}^{-2} / 5\text{ mA h cm}^{-2}$ for 10 h. As the cycling time went by (after 25 h), more protrusions were formed on the bare Li, resulting in several huge porous dendrites. Compared to bare Li, dendritic structures or

fragmentation are not seen in the morphology of COF-Li even after cycling for 50 h, demonstrating that COF can effectively protect Li from dendrite growth.

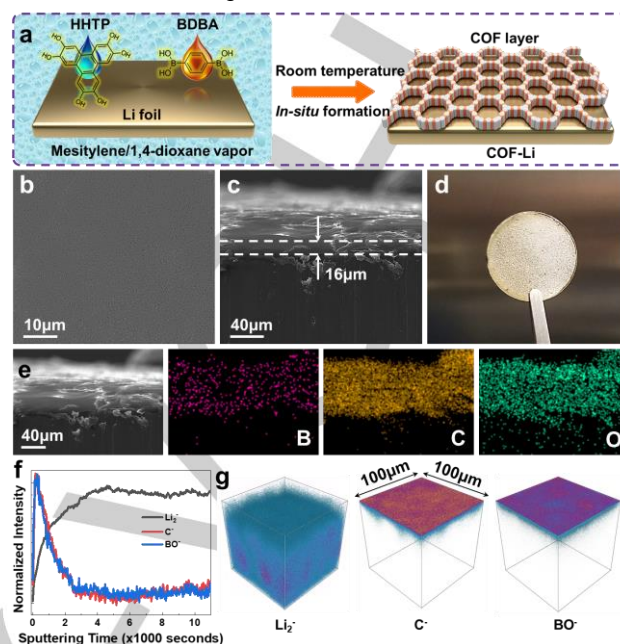


Figure 1. (a) Schematic of the synthesis route for COF-Li. (b) Top-surface and (c) Cross-sectional morphologies of COF-Li. (d) A digital photo of COF-Li. (e) Cross-sectional morphologies of COF-Li, and the corresponding elemental mapping images of boron, carbon, and oxygen. (f) Depth profiles of Li_2^+ , C^+ , and BO^+ secondary ions in fresh COF-Li. (g) 3D visualization of the architectural evolution of COF-Li.

To examine the cycling stability of COF-Li anode, comparative voltage profiles are shown in Figure 2b, which demonstrate the Li plating/stripping behaviors of COF-Li and bare Li in symmetric cells at $5\text{ mA cm}^{-2} / 5\text{ mA h cm}^{-2}$. The overpotential of the cell with bare Li is initially $> 680\text{ mV}$, and then dramatic voltage changes occur as early as 60 h of cycling, suggesting a cracking SEI and continuous corrosion on the bare Li. Impressively, the symmetric cell with COF-Li exhibits a low initial overpotential of only 33 mV and displays a remarkable cycle life of 1,200 h. To fully demonstrate the advantage of the COF in the protection of Li, the symmetric cell with COF-Li was further tested at a higher current density of 10 mA cm^{-2} and a higher areal capacity of 10 mA h cm^{-2} . As shown in Figure 2c, the symmetric cell with COF-Li shows a low overpotential of 53 mV at the initial cycle. More importantly, the COF-Li realizes a remarkable cycle life over 13,200 h with an impressive low overpotential of 16 mV. Such extraordinary lifespan is the longest compared to all the previous reports on Li-metal protection in the literature, fully demonstrating that COF can effectively protect the Li foil from dendrite growth with an ultra-stable SEI on Li. To investigate the evolution of the voltage profiles in detail, the 2,000th, 7,000th, and 12,000th cycles are zoomed in Figure 2d. The symmetric cell with COF-Li exhibits flat charge/discharge profiles with very low and stable overpotential with stable cycling performance, demonstrating that COF can construct a stable interface between the electrolyte and Li. The smooth surface of cycled COF-Li reconfirms the excellent protection of COF from Li dendrite growth, as evident in the SEM image in Figure S5. In sharp

contrast, many mossy dendritic Li can be detected on the surface of Li foil in the SEM image of the cycled bare Li (Figure S6). Another critical parameter to evaluate for the stability of a Li anode is the Coulombic efficiency (CE), which is defined as the ratio of Li stripping capacity to Li plating capacity. As shown in Figure S7, the COF-Cu delivers an initial CE of 97.7% and then remains stable and high at 98.6% over 200 cycles, under a high current density of 5 mA cm^{-2} . On the contrary, the CE of bare Cu begins at around 75.2% and fluctuates with a final dramatic drop after 108 cycles. Such results are in a sharp contrast and reconfirm that the COF-Li can effectively prevent the growth of Li dendrites and repetitive breakdown of SEI.

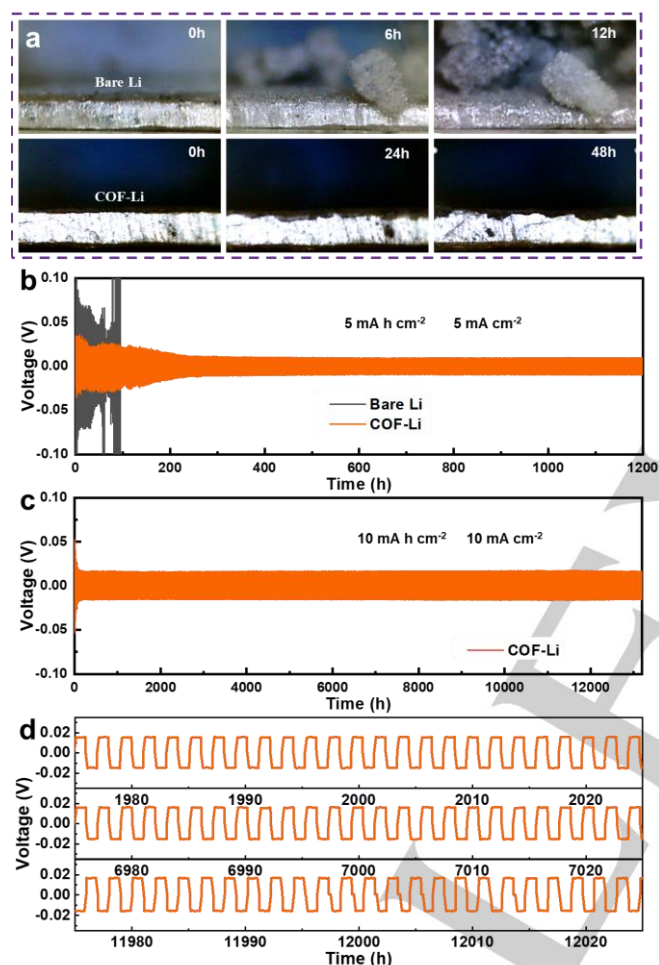


Figure 2. (a) *In situ* optical microscopy observations of the Li deposition process on COF-Li or bare Li. (b) Voltage profiles of Li plating/stripping in symmetric cells with COF-Li or bare Li at $5 \text{ mA cm}^{-2} / 5 \text{ mA h cm}^{-2}$. (c) Voltage profiles of Li plating/stripping in symmetric cells with COF-Li at $10 \text{ mA cm}^{-2} / 10 \text{ mA h cm}^{-2}$ and (d) its voltage-time curves at different times.

To further demonstrate that COF can selectively sieve Li ions, COF-Li was paired with a sulfur cathode using commercial Ketjen Black carbon as a sulfur host to avoid nano-scale effects from the designed nanostructures. As shown in Figure 3a, the cell with bare Li delivers a low initial capacity of 906 mA h g^{-1} , with a gradually decreasing cycling performance under a sulfur loading of 5.2 mg cm^{-2} and an electrolyte-to-sulfur ratio (E/S) of $7 \mu\text{L mg}^{-1}$ at C/10 rate. Specifically, the capacity of the cell with

bare Li decays to 128 mA h g^{-1} after 200 cycles. In addition, the CE of the cell with bare Li starts at 92.2% and continuously decreases to 87.5% due to intensive LiPS shuttling in the cell and deposition on Li anode, leading to huge active material loss. In sharp contrast, the cell with COF-Li delivers a high reversible capacity of $1,143 \text{ mA h g}^{-1}$ and exhibits excellent cyclic stability over 200 cycles. Additionally, the cell with COF-Li shows a high initial CE of 95.6% and maintains good stability over 200 cycles with 99.3%. The low capacity fade rate and high CE of the cell with COF-Li demonstrate that COF can selectively sieve Li ions and thus prevent active material loss.

In order to achieve high energy density, it is necessary to have a large loading of the active material as well as high areal capacities. Consequently, further cycling stability of the cells with COF-Li under realistic conditions with a high sulfur loading and low E/S ratio was performed at C/10 rate. As shown in Figure 3b, the cell with COF-Li with a sulfur loading of 6.8 mg cm^{-2} and an E/S ratio of $6 \mu\text{L mg}^{-1}$ at C/10 rate delivers a high initial capacity of $1,014 \text{ mA h g}^{-1}$, corresponding to an areal capacity of 6.9 mA h cm^{-2} , and exhibit stable cycling performance over 200 cycles with a high capacity retention of 86%. Surprisingly, when the sulfur loading increases to 8.7 mg cm^{-2} and the E/S ratio decreases to $5 \mu\text{L mg}^{-1}$, the COF-Li cell still delivers a high capacity of 830 mA h g^{-1} . In addition, even under such conditions, the cell maintains a stable cycling performance over 200 cycles with a peak capacity of 943 mA h g^{-1} , corresponding to an impressive areal capacity of 8.2 mA h cm^{-2} . It is noteworthy that such an excellent cycling performance is obtained under the conditions required for practical high-energy Li-S batteries: a high sulfur loading of 8.7 mg cm^{-2} and a low E/S ratio of $5 \mu\text{L mg}^{-1}$. Since long-term cycling is a critical part of cell evaluation, COF-Li was further tested to achieve a longer lifespan. As shown in Figure 3c, the cell with COF-Li delivers a high initial capacity of $1,055 \text{ mA h g}^{-1}$. It remains stable over 600 cycles with a capacity fade rate of only 0.05% per cycle at a high current density of 1C rate.

The evaluation of energy materials in a pouch cell is an essential aspect in probing the stability of the electrode and the performance of Li anode in order to realize practical Li-S batteries. As shown in Figure 3d, a pouch cell with COF-Li was tested at C/20 rate under the realistic condition with a high sulfur loading of 6 mg cm^{-2} , a lean electrolyte of $4.5 \mu\text{L mg}^{-1}$, and a low negative to positive electrode capacity ratio of 2.4. Impressively, the pouch cell with COF-Li exhibits excellent cyclic stability and remains stable over 40 cycles. For a comparison, the pouch cell with bare Li shows comparable capacity initially, but rapidly fades to a much lower capacity than the cell with COF-Li. The limited Li dendrite growth under low current density at the beginning of cycling results in the comparable capacity of both cells. Then, more and more uneven formation of Li dendrites and active material loss upon cycling leads to significant capacity fade in the pouch cell with bare Li. The dendritic Li growth and LiPS shuttling become more severe at higher current density. As shown in Figure 3e, the pouch cell with COF-Li delivers much higher capacity and exhibits more stable cycling performance over 31 cycles than bare Li at C/10 rate.

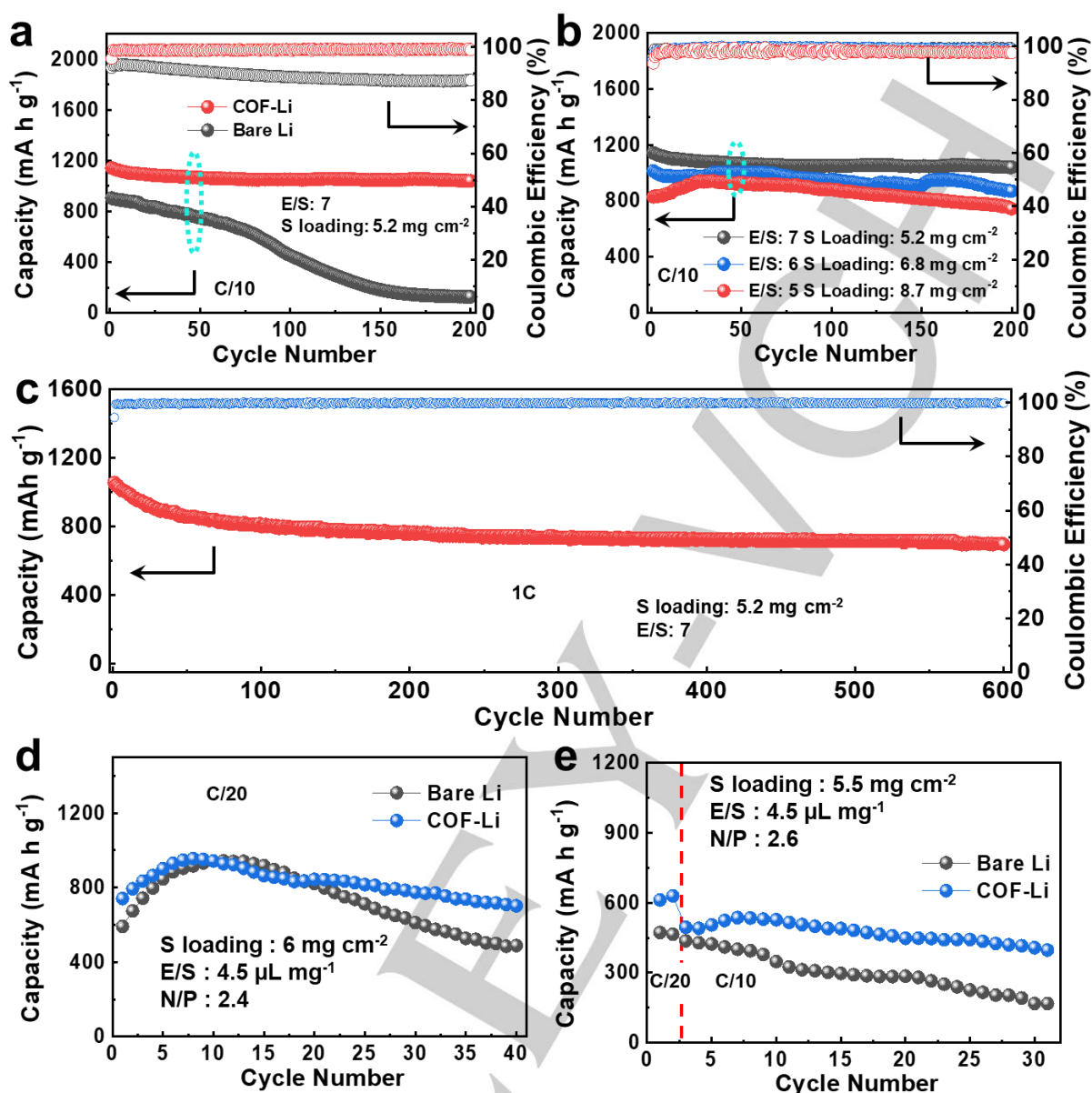


Figure 3. (a) Cyclic stability of the Li-S cells with COF-Li and bare Li at C/10 rate for 200 cycles. (b) Cycling performances of the cells with COF-Li at C/10 rate with various sulfur loadings. (c) Long-term cycle life and corresponding Coulombic efficiency of Li-S cell with COF-Li. (d) Cycling stability of Li-S pouch cells with COF-Li and bare Li at a C/20 rate. (e) Cycling stability of Li-S pouch cells with COF-Li and bare Li at C/20 and C/10 rates.

To gain a deep insight into the improved performance of the cell with COF-Li, ToF-SIMS on the cycled anode was carried out. As shown in Figure 4a, the depth profiles of the representative secondary-ion species reveal the composition of the cycled bare Li paired with a sulfur cathode, which are Li_2^+ , BO^+ , LiS^+ , and SO^+ . Here, Li_2^+ , BO^+ , LiS^+ , and SO^+ secondary ions are, respectively, representative of metallic lithium, COF, Li_2S , and oxidized sulfur species (such as Li_2SO_4). It can be seen from the depth profiles that the signal for Li_2^+ exhibits no initial peak at all, but instead it gradually increases to reach a stable level at the end of sputtering. This implies the formation of an SEI layer comprised of lithium-electrolyte reaction products on top of metallic lithium after long-term cycling, consistent with previous findings.^[13] The composition of the SEI layer was revealed to be Li_2S , oxidized sulfur species, and others. The LiS^+ and SO^+ signals exhibit an initial peak and subsequently decrease to reach a steady level

with increasing depth. Such a result reconfirms thick SEI formation on metallic lithium. The 3D visualization of the architecture evolution of the cycled bare Li in Figure 4c demonstrates that such thick SEI composites do not form a uniform layer on the top surface. Also, the depletion of lithium inventory is illustrated in Figure 4c, in which very limited Li_2^+ can be detected. Moreover, these thick inactive species trap metallic lithium tightly, which is similar to some of the isolated pockets of metallic lithium in the bulk, depriving access to Li ions and electrons and are considered as “dead.”^[14]

In sharp contrast, the representative secondary-ion species of cycled COF-Li show different behaviors, consisting of four layers. As shown in Figure 4b, the signal for Li_2^+ also exhibits no initial peak, but instead shows a gradual increase to reach a stable level after sputtering for 7,000 s. The signal for BO^+ shows no initial rise, but rapidly increases after sputtering for 500 s,

reaches a peak, and subsequently falls off quickly to a stable value after 7,000 s, reconfirming that the COF tightly coats on metallic lithium. The signal for LiS^+ shows an initial peak and drops off rapidly after sputtering 500 s, indicating that the COF layer has effectively blocked the LiPSs or lithium sulfide species. The signal for SO^- shows a maximum signal intensity at the beginning and rapidly drops off, suggesting limited oxidized sulfur species on the cycled COF-Li. The 3D visualization of the architecture evolution in Figure 4d demonstrates the four-layer structure of the cycled COF-Li. The COF layer protects metallic lithium from LiPSs or lithium sulfides species. Therefore, a lot of Li_2^- underneath can be detected. It is noteworthy that the SO^- layer is skinny in Figure 4d, suggesting a minimally oxidized sulfur species on the cycled COF-Li. All the sulfur species on cycled bare Li and COF-Li were further investigated by X-ray photoelectron spectroscopy (XPS). As shown in Figure S8, the intensively oxidized sulfur species can be detected on the surface of cycled bare Li instead of COF-Li, matching well with ToF-SIMS results. The cross-sectional SEM further confirms the thick SEI and other inactive species on the cycled bare Li in Figure 4e. Over 200 μm thick layer can be observed on Li with a mossy morphology. In contrast, the cycled COF-Li still maintains a smooth surface with a very thin coating layer. As shown in Figure 4f, the thickness of cycled COF layer was 28 μm , which was nearly 2 times that of a fresh COF layer (16 μm). Such a volumetric expansion could be attributed to the deposition of small amount of Li_2S , which was demonstrated by the ToF-SIMS result in Figure 4d.

Based on the above discussion, the reason for the capacity fade of traditional Li-S batteries in the anode region can be explained as shown in Figure 4g: (i) Intensive LiPSs formation and direct deposition of lithium sulfides on the anode leads to their trapping within the anode resulting in huge active material loss. (ii) The lithium sulfide deposited on Li-metal has direct access to electrons, thus promoting polysulfide shuttle. (iii) Thick, inactive, and uneven coating on metallic lithium forms a tremendous amount of "dead" lithium. (iv) Li dendrite growth increases the surface area of the repetitively deposited lithium, resulting in severe side reactions that consume a large amount of electrolyte. Compared to the bare Li, the COF-Li has several advantages, as shown in Figure 4h: (i) lithium sulfides deposited on the COF can be effectively reutilized by dissolved polysulfides through disproportionation, thus reducing active material loss. (ii) Electrical disconnection of the lithium sulfides from Li metal prevents electron exchange and thus the shuttle. (iii) Preventing inactive species formation, including oxidized sulfur species, can enhance the utilization of Li. (iv) Suppression of Li dendrite growth and avoiding direct contact of organic electrolyte with Li can reduce the consumption of electrolyte. This demonstrates that an electrically disconnected lithium sulfide-rich SEI facilitated by a thin, ion-sieving, electron-blocking, mechanically robust COF layer on Li-metal is ideally suited for the polysulfide-rich environment of Li-S batteries.

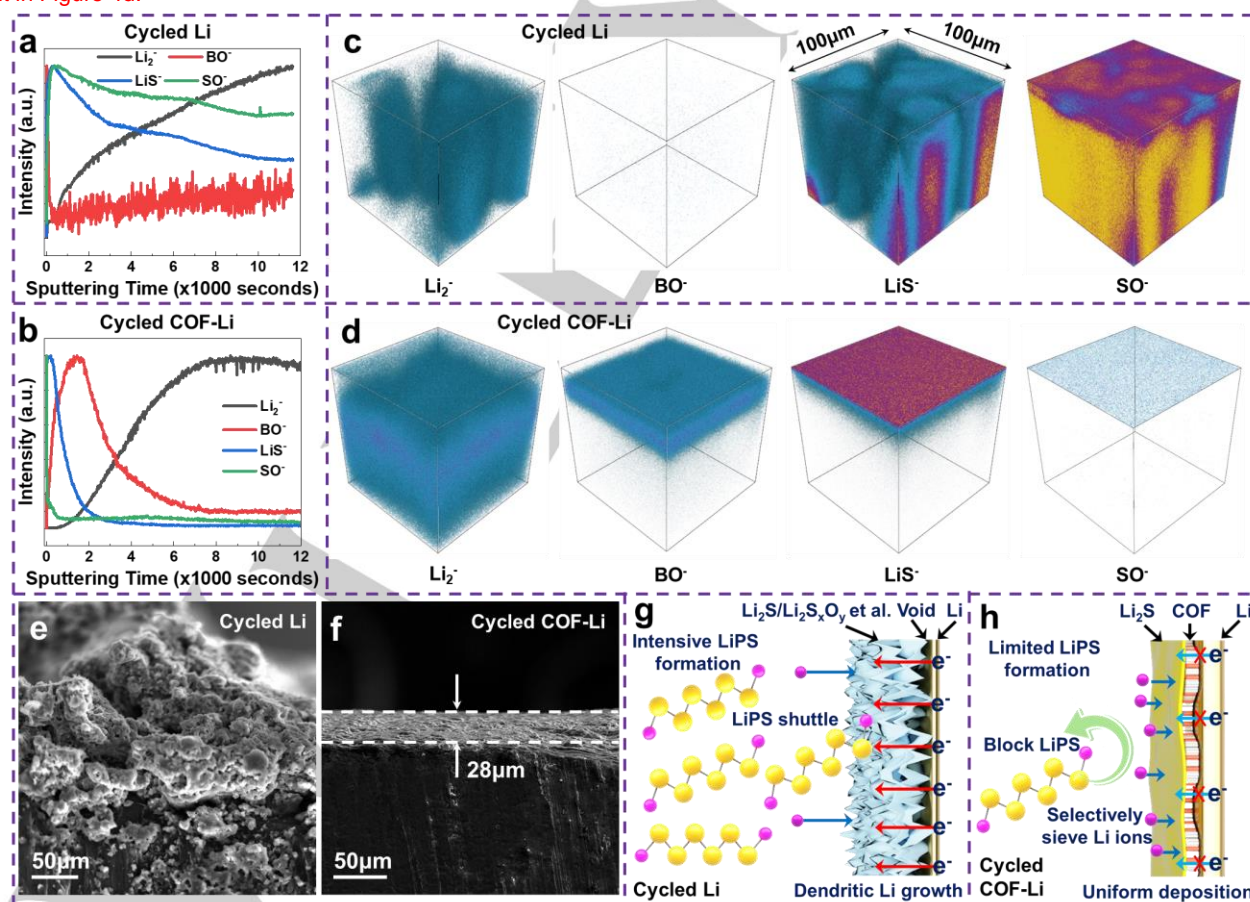


Figure 4. Depth profiles for Li_2^- , BO^- , LiS^+ and SO^- secondary ions in (a) cycled Li and (b) cycled COF-Li. 3D visualization of (c) cycled Li and (d) cycled COF-Li architecture evolution. Cross-sectional morphologies of (e) cycled Li and (f) cycled COF-Li. Schematic of the Li SEI structure in (g) cycled Li and (h) cycled COF-Li.

Conclusion

In conclusion, COF is demonstrated to be an efficient protective layer for a stable Li-metal anode. When the *in-situ* prepared COF-Li serves as an anode in Li-S batteries, it shows several advantages under more complex working conditions. First, COF-Li protects lithium from direct deposition of lithium sulfides, effectively improving sulfur utilization. Second, COF-Li prevents inactive species formation, including oxidized sulfur species, which helps enhance the utilization of Li. Finally, COF effectively suppresses Li dendrite growth and avoids direct contact of organic electrolyte with Li, reducing the consumption of electrolyte. The approach highlights the importance of selectively sieving Li ions and effectively protecting the Li anode under complex working conditions. This work paves a new path forward to Li-anode protection and is also instructive for other metal batteries with complex working conditions.

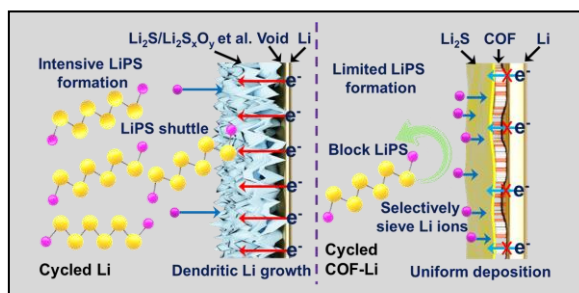
Acknowledgements

This work was supported by the U.S. Department of Energy, Office of Basic Energy Sciences, Division of Materials Science and Engineering under award number DE-SC0005397.

Keywords: lithium-metal batteries • artificial interphase • covalent organic framework • dendrite-free anode • electrochemistry

- [1] a) A. Bhargav, A. Manthiram, *Adv. Energy Mater.* **2020**, 2001658; b) H. Gao, L. Xue, S. Xin, J. B. Goodenough, *Angew. Chem. Int. Ed.* **2018**, *57*, 5449; c) S. Nanda, A. Bhargav, A. Manthiram, *Joule* **2020**, *4*, 1121; d) A. Manthiram, *Nat. Commun.* **2020**, *11*, 1550; e) J. He, A. Bhargav, H. Yaghoobnejad Asl, Y. Chen, A. Manthiram, *Adv. Energy Mater.* **2020**, *10*, 2001017.
- [2] a) W. J. Chen, B. Q. Li, C. X. Zhao, M. Zhao, T. Q. Yuan, R. C. Sun, J. Q. Huang, Q. Zhang, *Angew. Chem. Int. Ed.* **2020**, *59*, 10732; b) R. Zhang, X. Chen, X. Chen, X. Cheng, X. Zhang, C. Yan, Q. Zhang, *Angew. Chem. Int. Ed.* **2017**, *56*, 7764; c) D. Zhou, A. Tkacheva, X. Tang, B. Sun, D. Shanmukaraj, P. Li, F. Zhang, M. Armand, G. Wang, *Angew. Chem. Int. Ed.* **2019**, *58*, 6001.
- [3] a) Y. Guo, H. Li, T. Zhai, *Adv. Mater.* **2017**, *29*, 1700007; b) L. Liu, Y. Yin, J. Li, S. Wang, Y. Guo, L. Wan, *Adv. Mater.* **2018**, *30*, 1706216; c) B. Zhu, Y. Jin, X. Hu, Q. Zheng, S. Zhang, Q. Wang, J. Zhu, *Adv. Mater.* **2017**, *29*, 1603755; d) D. Chen, Y. Liu, C. Xia, Y. Han, Q. Sun, X. Wang, W. Chen, X. Jian, W. Lv, J. Ma, W. He, *InfoMat* **2021**, 12247; e) C. J. Zhang, L. Cui, S. Abdolhosseinzadeh, J. Heier, *InfoMat* **2020**, *2*, 613.
- [4] a) X. Liu, J. Liu, T. Qian, H. Chen, C. Yan, *Adv. Mater.* **2019**, *32*, 1902724; b) G. Huang, J. Han, F. Zhang, Z. Wang, H. Kashani, K. Watanabe, M. Chen, *Adv. Mater.* **2019**, *31*, 1805334; c) S. Liu, X. Xia, S. Deng, D. Xie, Z. Yao, L. Zhang, S. Zhang, X. Wang, J. Tu, *Adv. Mater.* **2018**, *31*, 1806470.
- [5] a) C. Yan, X. Cheng, Y. Tian, X. Chen, X. Zhang, W. Li, J. Huang, Q. Zhang, *Adv. Mater.* **2018**, *30*, 1707629; b) Z. Jiang, Z. Zeng, X. Liang, L. Yang, W. Hu, C. Zhang, Z. Han, J. Feng, J. Xie, *Adv. Funct. Mater.* **2020**, 2005991.
- [6] a) Z. L. Brown, S. Heiskanen, B. L. Lucht, *J. Electrochem. Soc.* **2019**, *166*, A2523; b) Q. Dong, B. Hong, H. Fan, H. Jiang, K. Zhang, Y. Lai, *ACS Appl. Mater. Inter.* **2019**, *12*, 627; c) Z. Yu, H. Wang, X. Kong, W. Huang, Y. Tsao, D. G. Mackanic, K. Wang, X. Wang, W. Huang, S. Choudhury, Y. Zheng, C. V. Amanchukwu, S. T. Hung, Y. Ma, E. G. Lomeli, J. Qin, Y. Cui, Z. Bao, *Nature Energy* **2020**, *5*, 526; d) J. He, A. Bhargav, W. Shin, A. Manthiram, *J. Am. Chem. Soc.* **2021**, *143*, 20241; e) J. He, A. Bhargav, A. Manthiram, *Adv. Energy Mater.* **2021**, *12*, 2103204.
- [7] N. W. Li, Y. X. Yin, C. P. Yang, Y. G. Guo, *Adv. Mater.* **2016**, *28*, 1853.
- [8] J. Qian, W. A. Henderson, W. Xu, P. Bhattacharya, M. Engelhard, O. Borodin, J. G. Zhang, *Nat. Commun.* **2015**, *6*, 6362.
- [9] D. D. Medina, J. M. Rotter, Y. Hu, M. Dogru, V. Werner, F. Auras, J. T. Markiewicz, P. Knochel, T. Bein, *J. Am. Chem. Soc.* **2015**, *137*, 1016.
- [10] D. A. Vazquez-Molina, G. S. Mohammad-Pour, C. Lee, M. W. Logan, X. Duan, J. K. Harper, F. J. Uribe-Romo, *J. Am. Chem. Soc.* **2016**, *138*, 9767.
- [11] H. Li, J. Brédas, *Chem. Mater.* **2021**, *33*, 4529.
- [12] D. Chen, S. Huang, L. Zhong, S. Wang, M. Xiao, D. Han, Y. Meng, *Adv. Funct. Mater.* **2019**, 1907717.
- [13] S. Nanda, A. Manthiram, *Adv. Energy Mater.* **2021**, *11*, 2003293.
- [14] a) S. Nanda, A. Manthiram, *Energ. Environ. Sci.* **2020**, *13*, 2501; b) S. Nanda, A. Bhargav, Z. Jiang, X. Zhao, Y. Liu, A. Manthiram, *Energ. Environ. Sci.* **2021**, *14*, 5423.

Entry for the Table of Contents



A thin covalent organic framework layer is *in-situ* fabricated on Li (COF-Li) to suppress Li dendrite growth and mitigate side reactions on Li anode. COF-Li exhibits a non-dendritic morphology during repeated Li plating/stripping and demonstrates a remarkable cycle life of > 13,200 h with an impressive low overpotential of 16 mV at a high current density of 10 mA cm^{-2} and a high areal capacity of 10 mA h cm^{-2} .

Institute and/or researcher Twitter usernames: @Manthiram_UT